ENVIRONMENTAL RESEARCH
LETTERS

LETTER • OPEN ACCESS

The scenario-based variations and causes of future surface soil moisture across China in the twenty-first century

To cite this article: Keke Fan *et al* 2021 *Environ. Res. Lett.* **16** 034061

ENVIRONMENTAL RESEARCH
LETTERS

OPEN ACCESS

RECEIVED
18 May 2020

REVISED
15 January 2021

ACCEPTED FOR PUBLICATION
21 January 2021

PUBLISHED
8 March 2021

LETTER

The scenario-based variations and causes of future surface soil moisture across China in the twenty-first century

Keke Fan[1,2,3], **Qiang Zhang**[1,2,3], **Jianping Li**[4], **Deliang Chen**[5] **and Chong-Yu Xu**[6]

[1] Key Laboratory of Environmental Change and Natural Disaster, Ministry of Education, Beijing Normal University, Beijing 100875, People's Republic of China
[2] State Key Laboratory of Earth Surface Processes and Resource Ecology, Beijing Normal University, Beijing 100875, People's Republic of China
[3] Faculty of Geographical Science, Academy of Disaster Reduction and Emergency Management, Beijing Normal University, Beijing 100875, People's Republic of China
[4] Key Laboratory of Physical Oceanography, Ministry of Education, Ocean University of China, Qingdao 266100, People's Republic of China
[5] Regional Climate Group, Department of Earth Sciences, University of Gothenburg, Box 460, SE-405 30 Gothenburg, Sweden
[6] Department of Geosciences and Hydrology, University of Oslo, P O Box 1047 Blindern, N-0.16 Oslo, Norway

E-mail: zhangq68@bnu.edu.cn

Keywords: surface soil moisture, spatiotemporal evolution, climate scenarios, hydrological cycle

Abstract

Surface soil moisture (SSM) is a key factor for water and heat exchanges between land surface and the atmosphere. It is also important to water resources, agriculture, and ecosystems. In the backdrop of global warming, SSM variations and potential causes are not well-known at regional scales. Based on soil moisture (SM) data from GLDAS-Noah and 16 global climate models (GCMs) selected from 25 GCMs in CMIP5, we analyzed spatial distribution and temporal changes of SSM in China and quantified fractional contributions of four meteorological factors to the SSM variations. The selected models have the same direction of historic trends in SSM during 1981–2005 as those in the GLDAS SSM data which were also further used to calibrate the trends simulated by the 16 GCMs. Based on the calibration results for the 16 GCMs, future SSMs for nine regions were analyzed in mainland China under four Intergovernmental Panel on Climate Change emission scenarios. No significant changes were identified in SSM across most regions of mainland China under RCP2.6 scenario. However, there is a general wetting tendency in the arid regions and drying tendency across the humid regions under all the scenarios except RCP2.6. In general, the higher the global temperature raises, the more grids with significant increase or significant decrease in SSM. These findings contradicted prevailing view that wet regions get wetter and dry regions get drier. Attribution analysis indicates that precipitation acts as the major driver for SSM variations and contributes up to 43.4% of SSM variations across China. These results provide new insights into future SSM response to climate warming and a scientific basis to mitigation and adaptation works related to SSM in the future.

1. Introduction

Surface soil moisture (SSM) is a pivotal variable of the terrestrial system and plays a critical role in energy exchange and hydrological cycle (Brocca *et al* 2012, Miralles *et al* 2014, Berg *et al* 2017, McColl *et al* 2017), mainly through its control on the partitioning of radiation and evapotranspiration at the surface (Albergel *et al* 2013, Fan *et al* 2019). Furthermore, SSM also plays a critical role in hydro-climatic extreme events (Miralles *et al* 2019), vegetation changes (Chen *et al* 2014) and physical properties of soil (Gunda *et al* 2017). Soil moisture (SM) is also a state variable controlling surface runoff, soil drainage, and soil-freeze-thaw status (Zhang *et al* 2015), and for other hydrological, meteorological and ecological applications (Cui *et al* 2019). As a consequence, the Global Climate Observing System (GCOS) Programme recognizes SM as an essential climate variable (ECV) (Albergel *et al* 2013, Zhang *et al* 2019).

Recent years witnessed an increasing availability of datasets of SM sourced from satellite

remote sensing and assimilation technologies (Miralles *et al* 2010, Zhang *et al* 2018, Gu *et al* 2019). The remotely sensed data products such as those from the Advanced Microwave Scanning Radiometer for Earth Observing System (AMSR-E and AMSR-2), the Advanced Scatterometer (ASCAT), the Soil Moisture Ocean Salinity or the Soil Moisture Active Passive, and from the European Space Agency Climate Change Initiative were widely used. A limitation of these datasets is that they provide only near-surface (∼0–5 cm) SM estimates (Zohaib *et al* 2017, Zhang *et al* 2018). For this reason, assimilation technologies were employed to derive SM estimates from multiple soil layers, such as the European Centre for Medium-Range Weather Forecasts atmospheric reanalysis (ERA), The Global Land Data Assimilation System (GLDAS), the Modern-Era Retrospective analysis for Research and Application (MERRA), which were also widely used as alternatives for 'true value' (Deng *et al* 2020). In addition, GLDAS has been used to study global and regional SM trends (Dorigo *et al* 2012, Zhang *et al* 2018, 2019, Gu *et al* 2019).

SM changes can be influenced by numerous factors such as human activities (Samaniego *et al* 2018) like irrigation (Yu *et al* 2019) and climate changes such as changes in precipitation and temperature (Feng and Liu 2015, Gunda *et al* 2017, Guillod *et al* 2015, Hauser *et al* 2016). Temperature directly affects the loss of SM to the atmosphere by influencing evapotranspiration processes, while precipitation provides inputs to SM (Varallyay 2010, Gunda *et al* 2017). According to the Fifth Assessment Report (AR5) by the Intergovernmental Panel on Climate Change (IPCC), global warming has become indisputable and is caused mainly by human activities (Stocker *et al* 2013). Global warming heavily affects hydrological cycles and water balances at different spatial scales, modifying spatiotemporal patterns of water resources (Berg *et al* 2017). As an example, mounting evidences indicate that increased continental precipitation and evapotranspiration most likely lead to decreased SM in a warming climate, although regional differences exist (Feng and Liu 2015, Zhao and Dai 2015, Huang *et al* 2016).

SM can influence crop yields directly by modulating the plant-available water (Wang *et al* 2011). China is the world's largest agricultural producer and has the world's largest population. Because of the importance of water resources and agricultural development to China's economy and people, the relationships between extreme weather events, floods, and droughts, and agricultural production have been intensively studied (Zhang *et al* 2015, 2017). In particular, it is critical for China to bridge the knowledge gap between climate changes and SM variations in both space and time (Koster *et al* 2004 Fan *et al* 2019). Currently, there are limited studies of SM changes and related causes in China. Wang *et al* (2011) employed four physically based land surface hydrology models to explore the characteristics of SM drought in China during 1950–2006 and found SM in southeastern and northeastern China were drying significantly. Chen *et al* (2016a and 2016b) found a significant drying trend of SSM in Eastern China and explored the spatiotemporal SSM changes across China in responses to climate in the 1979–2010 period. Previous studies focused on the causes of SSM changes during the historical period only.

Characteristics of future SM are rarely explored in previous studies. Besides, it still remains a challenge to quantify how SM changes at regional scale due to substantial spatial heterogeneity of SM variations (e.g. Wang 2005). Therefore, in this study, we first used GLDAS-Noah SM dataset to assess the historical simulations of global climate models (GCMs) in CMIP5 and selected GCMs with the consistent trend to GLDAS-Noah for better reliability of future projections. Then we employed the SM median of chosen GCMs in CMIP5 as projected SM to investigate the characteristics and causes of future SM changes that can help predict agricultural drought across China during historical and future periods.

2. Study region and data

Given the distinct spatial heterogeneity of meteorological variables and SM over mainland China (CHN) was subdivided into nine regions (figure 1), i.e. Northeast China (NEC); North China (NCH); Central China (CCH); South China (SCH); Southwest China (SWC); the eastern part of Northwest China (ENW); the central part of Northwest China (CNW); the western part of Northwest China (WNW); Tibet Plateau (TPC). In order to investigate the effects of potential driving factors on SSM at the regional scale, we divided the area into regular rectangles to further minimize the errors sourced from the reduced number of grids in marginal areas (table 1, totally 1062 grids across China). Generally, NEC, NCH, CCH, SCH, SEC mostly locate in the monsoon area in the eastern China; ENW, CNW, WNW mostly situate in the arid and semi-arid areas in the northwestern China, and TPC is approximately in the Tibetan Plateau high-cold area (Xiao *et al* 2013).

We selected SM outputs of 25 GCM models from Coupled Model Intercomparison Project Phase 5 (CMIP5) in historical and future periods under historical forcing and RCP2.6, RCP4.5, RCP6.0 and RCP8.5 scenarios (table 2). The monthly SM dataset was sourced from the ESGF (the Earth System Grid Federation) node (https://esgf-data.dkrz.de/search/cmip5-dkrz/). The outputs of models considered in this study include at least two future scenarios in both the uppermost 10 cm soil layer and root-zone soil layers. Meanwhile, the models chosen in this study are with the ensemble of r1i1p1 and only the data from output1 was accepted (Taylor *et al* 2012). Moreover, the monthly data

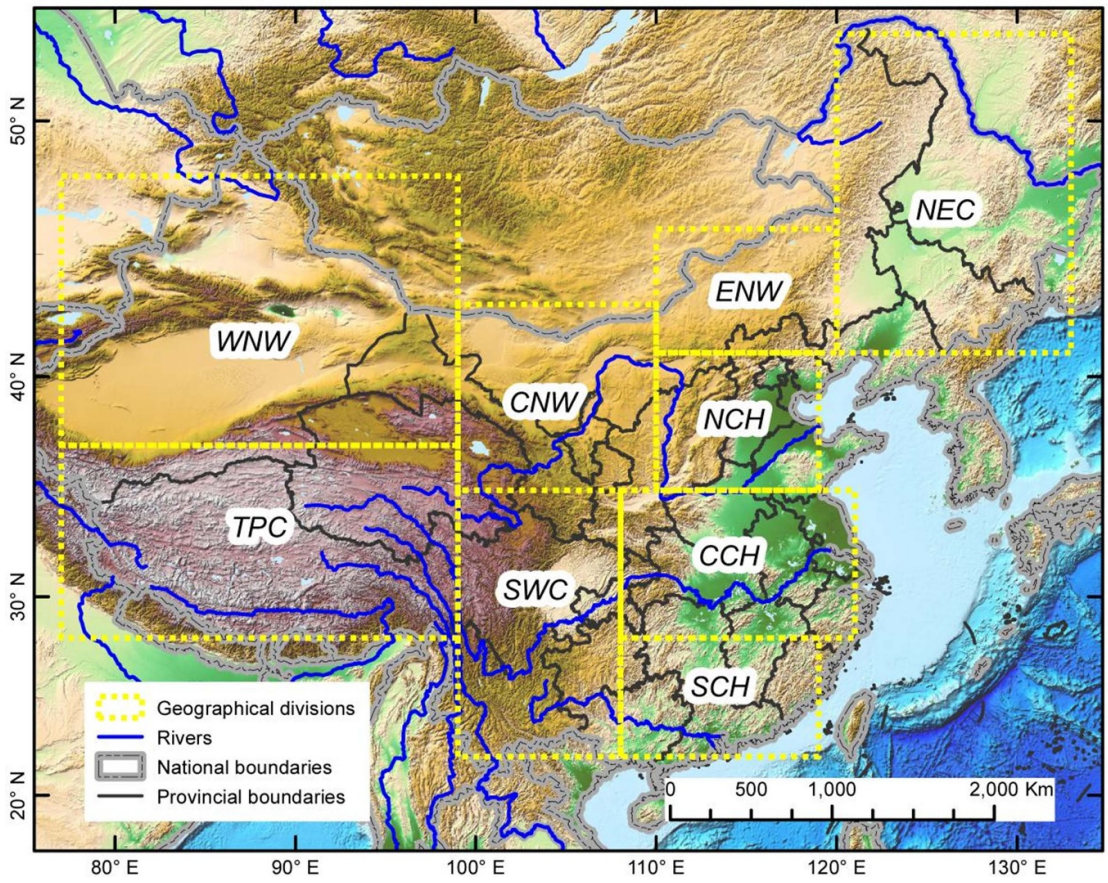

Figure 1. Relief and geographical division map across China. Mainland China (CHN) is subdivided into nine sub-regions which are marked with Acronyms: NEC (Northeastern China); NCH (Northern China); CCH (Central China); SCH (Southern China); SWC (Southwestern China); ENW (the east part of Northwestern China); CNW (the central part of Northwestern China); WNW (the west part of Northwestern China); TPC (Tibet Plateau). According to the most commonly used geographic (mainly climatic) divisions, NEC, NCH, CCH, SCH, SEC are located mainly in the monsoon climate area in the East China; ENW, CNW, WNW are mostly situated in the arid and semi-arid areas in the northwestern China; and the TPC is approximately the Tibetan Plateau high-cold area.

Table 1. Coordinates of corners of nine different regions around China. The nine regions are defined in the standard rectangular meshes which can be found in figure 1.

No	Region	Acronym	Left-bottom	Right-top	Grid No. (1° × 1°)	Percent in total area of CHN
1	Northeastern China	NEC	120 E, 41 N	133 E, 53 N	156	14.7%
2	Northern China	NCH	110 E, 35 N	120 E, 41 N	54	5.1%
3	Central China	CCH	108 E, 28 N	121 E, 35 N	91	8.6%
4	Southern China	SCH	108 E, 22 N	119 E, 28 N	66	6.2%
5	Southwestern China	SWC	99 E, 22 N	108 E, 35 N	117	11.0%
6	East part of Northwestern China	ENW	110 E, 41 N	120 E, 46 N	50	4.7%
7	Central part of Northwestern China	CNW	99 E, 35 N	110 E, 43 N	88	8.3%
8	West part of Northwestern China	WNW	77 E, 37 N	99 E, 48 N	242	22.8%
9	Tibet Plateau	TPC	77 E, 28 N	99 E, 37 N	198	18.6%

of climate variables, including precipitation, 2 m air temperature, wind speed and relative humidity from the CMIP5 outputs were also analyzed to quantify climatic effects on SM.

The Global Land Data Assimilation System (GLDAS) was developed to generate optimal fields of land surface states and fluxes by integrating satellite- and ground-based observed data products, using land surface modeling and data assimilation techniques (Rodell *et al* 2004). GLDAS drives four models, including Noah, Mosaic, VIC and CLM, which are sourced from the Goddard Earth Sciences Data and Information Services Center (http://disc.sci.gsfc.nasa.gov/hydrology/data-holdings). Noah simulates SM outputs of four layers (0–10 cm, 20–40 cm, 40–100 cm and 100–200 cm). In this study, Noah V2.0 with spatial resolution of 0.25° × 0.25° and time interval of 1948–2010 can

Table 2. 25 GCM models from CMIP5 with modelling results of the soil moisture under historical forcing and future scenarios. These models include at least two future scenarios. The date refers to the time range covering the whole data sets at monthly scale but only the period of up to 2100 years was analyzed.

No.	Model name	Institute ID	Resolution (longitude × latitude)	Historical	RCP2.6	RCP4.5	RCP6.0	RCP8.5	Soil depth (meter)
1*	ACCESS1.0	CSIRO-BOM	192 × 145	185 001–200 512	×	200 601–210 012	×	200 601–210 012	3
2	ACCESS1.3	CSIRO-BOM	192 × 145	185 001–200 512	×	200 601–210 012	×	200 601–210 012	4.6
3*	CanESM2	CCCMA	128 × 64	185 001–200 512	200 601–230 012	200 601–230 012	×	200 601–210 012	4
4	CSIRO-Mk3.6.0	CSIRO-QCCCE	192 × 96	185 001–200 512	200 601–210 012	200 601–230 012	200 601–210 012	200 601–230 012	4.6
5*	FGOALS-g2	LASG-GESS	128 × 60	185 001–200 612	200 601–210 112	×	×	200 601–210 112	3.6
6*	FGOALS-s2	LASG-IAP	128 × 108	185 001–200 512	200 601–210 012	×	200 601–210 012	200 601–210 012	3.6
7*	GFDL-CM3	NOAA-GFDL	144 × 90	186 001–200 512	200 601–210 012	200 601–210 012	200 601–210 012	200 601–210 012	10
8*	GFDL-ESM2G	NOAA-GFDL	144 × 90	186 101–200 512	200 601–210 012	200 601–210 012	200 601–210 012	200 601–210 012	10
9*	GFDL-ESM2M	NOAA-GFDL	144 × 90	186 101–200 512	200 601–210 012	200 601–210 012	200 601–210 012	200 601–210 012	10
10*	GISS-E2-H	NASA-GISS	144 × 90	185 001–200 512	200 601–230 012	200 601–230 012	200 601–210 012	200 601–230 012	3.5
11*	GISS-E2-H-CC	NASA-GISS	144 × 90	185 001–201 012	×	200 601–210 012	×	200 601–210 012	3.5
12	GISS-E2-R	NASA-GISS	144 × 90	185 001–200 512	200 601–230 012	200 601–230 012	200 601–210 012	200 601–230 012	3.5
13*	GISS-E2-R-CC	NASA-GISS	144 × 90	185 001–201 012	×	200 601–210 012	×	200 601–210 012	3.5
14	HadGEM2-CC	MOHC	192 × 145	185 912–200 511	×	200 512–210 012	×	200 512–210 012	3
15*	HadGEM2-ES	MOHC	192 × 145	185 912–200 511	200 512–229 912	200 512–229 912	200 512–209 911	200 512–229 912	3
16*	INM-CM4	INM	180 × 120	185 001–200 512	×	200 601–210 012	×	200 601–210 012	10
17*	IPSL-CM5A-LR	IPSL	96 × 96	185 001–200 512	200 601–230 012	200 601–230 012	200 601–210 012	200 601–230 012	3.9
18*	IPSL-CM5A-MR	IPSL	144 × 143	185 001–200 512	200 601–210 012	200 601–230 012	200 601–210 012	200 601–210 012	3.9
19	IPSL-CM5B-LR	IPSL	96 × 96	185 001–200 512	×	200 601–210 012	×	200 601–210 012	3.9
20	MIROC5	MIROC	256 × 128	185 001–201 212	200 601–230 012	200 601–210 012	200 601–210 012	200 601–210 012	14
21	MIROC-ESM	MIROC	128 × 64	185 001–200 512	200 601–210 012	200 601–230 012	200 601–210 012	200 601–210 012	14
22	MIROC-ESM-CHEM	MIROC	128 × 64	185 001–200 512	200 601–210 012	200 601–210 012	200 601–210 012	200 601–210 012	14
23*	MRI-CGCM3	MRI	320 × 260	185 001–200 512	200 601–210 012	200 601–210 012	200 601–210 012	200 601–210 012	10
24*	NorESM1-M	NCC	144 × 96	185 001–200 512	200 601–210 012	200 601–230 012	200 601–210 012	200 601–210 012	43.8
25	NorESM1-ME	NCC	144 × 96	185 001–200 512	200 601–210 112	200 601–210 212	200 601–210 112	200 601–210 012	43.8

The resolution is referred to as the number of grids along the longitude and latitude. Asterisk (*): the model has been selected to conduct further analysis. Cross symbol (×): data are not available.

meet the requirement in spatial resolution at the regional scale and time length of validating modelled SM data in CMIP5. The Noah V2.0 used in this study covered the period of 1981–2005 and has been used widely in SM analysis (Zhang *et al* 2018, 2019, Gu *et al* 2019).

3. Methods

3.1. Pre-processing of the SM

In this study, hydrologically active soil depth varies from 3 to 14 m for GCMs (table 2) and only the first ten layers, down to 3.8 m for NorESM1 model are hydrological active (Lawrence *et al* 2011, Berg *et al* 2017). For SSM, GLDAS-Noah and the outputs of GCMs in CMIP5, which have been integrated over uppermost 10 cm, has the same surface soil depth. As a result, SSM is quantitatively comparable. Correspondingly, the deeper SM content varies widely due to obviously different SM depth. Given that GLDAS-Noah have maximum depth of 2 m and we focused more on SM changes of the upper SM column mostly accessible to ecosystems, we used SM outputs from CMIP5 to compute a 2 m SM content, which corresponds to the root-zone soil depth. Meanwhile, SM outputs were linearly interpolated to integrate the 2 m SM content for GCMs with the units of $m^3\ m^{-3}$ (Berg *et al* 2016). To reduce uncertainties and capture spatial patterns at regional scale, all SM variables were also resampled to a $1^\circ \times 1^\circ$ grid by bilinear interpolation before further analysis. All monthly data has been integrated into annual scale to explore the variation during the whole period. Then, we analyzed the relative SM changes in terms of the ratio (%) of the future (2005–2100) simulated mean SM change and the baseline mean SM during 1981–2005 rather than the absolute SM changes since that the SM changes are heavily model-dependent. Meantime, we normalized future SM where future-minus-present differences were divided by present simulated SM (Koster *et al* 2009, Berg *et al* 2016).

3.2. Verification and selection of GCMs in CMIP5

In this study, we adopted GLDAS-Noah SM data which has been widely used in SM analysis worldwide and for China as well (Dorigo *et al* 2012, Gu *et al* 2019, Liu *et al* 2019). Besides, we proposed the following indicator to show direction of trends at grid scales:

$$\mathrm{Ratio}_i = \frac{\mathrm{Trend}_{i2}}{\mathrm{Trend}_{i1}} \tag{1}$$

Wherein, i indicates the ith grid out of 1062 grids considered in this study; Trend_{i1} refers to the trend of the ith grid of the GLDAS-Noah SM data during 1981–2005; Trend_{i2} refers to the trend of the ith grid of the SM under historical scenarios during 1981–2005. The SM trends were calculated using the Sen's slope method by the 'trend' R package. Therefore, if Trend_{i1} and Trend_{i2} are positive or negative simultaneously, Ratio_i is positive, which indicates the prediction ability of the GCM in catching the direction of trend in the ith grid. Sixteen models with positive ratios in more than half of the total 1062 grids covering the entire study region were chosen for SSM, and the median SM of the simulated SM was used to explore SM variations.

Besides, magnitude of trends should also be normalized keeping consistency between magnitude of trends in SM by models and that by GLDAS-Noah dataset. In this case, we proposed a correction factor for this purpose, i.e. C_{trend}:

$$\mathrm{Trend}_{\mathrm{ic}} = \mathrm{Trend}_{im} \times C_{\mathrm{trend}} \tag{2}$$

wherein, Trend_{ic} indicates the calibrated SM trend of the ith grid for GCMs, Trend_{im} refers to the trend of the median SM in the ith grid for the chosen GCMs. The correlation factor is further used in the analysis under future scenarios. C_{trend} is calculated as:

$$C_{\mathrm{trend}} = \frac{\mathrm{Mean}(Abs(\mathrm{Trend}_{in}))}{\mathrm{Mean}(Abs(\mathrm{Trend}_{im}))} \tag{3}$$

wherein, Trend_{in} refers to the trend of the median SM in the ith grid for the GLDAS-Noah SM dataset. *Abs* refers to the absolute value function.

3.3. Attribution analysis with the geographic detector method

In this study, the attribution analysis was done using the geographic detector method that is a set of statistical methods that detect spatial differentiation and reveal the driving forces behind (Wang *et al* 2010). The major assumption behind geographic detector is that if an independent variable has an important influence on a dependent variable, the spatial pattern of the independent variable should be similar to that of the dependent variable. Geographic detectors method is adept at analyzing type quantities, and for sequential Quantities, ratios or intervals, as long as they are appropriately discretized (Cao *et al* 2013). Another unique advantage of Geodetector is to detect impacts of the interaction of two factors on the dependent variable. The general identification method of interaction is to add the product of two factors to the regression model to test its statistical significance. That is why we used Geodetector to quantify the effects of climate variables on SSM.

The geographic detector can determine whether there is interaction between two variables, and the strength, direction, linearity, or non-linearity of the interaction by calculating and comparing the single factor and the factor after the two factors are superimposed. The two-factor superposition includes both the multiplicative relationship and other relationships. As long as there is a relationship standing between two variables and this relationship

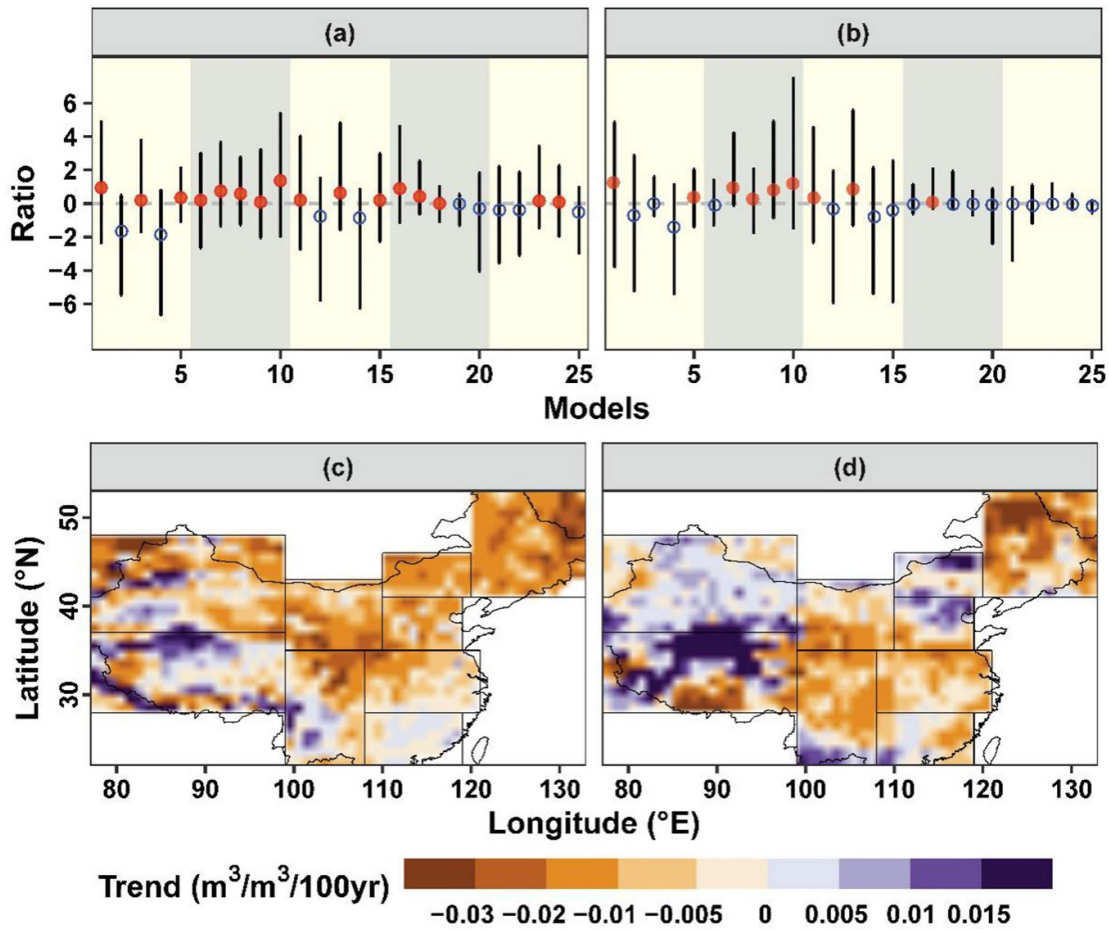

Figure 2. Comparison between the simulated SM with 25 CMIP5 GCMs and SM in the GLDAS-Noah dataset for 1981–2005. The upper panels show the ratio of the trends in CMIP5 GCMs to the trends in the GLDAS-Noah: (a) surface soil moisture; (b) root-zone soil moisture. The red solid points refer to the value >0 and the blue hollow points refer to the value <0. The *X*-axis is corresponding to the first column in table 2. (c) The lower panels show the spatial pattern of the GLDAS-Noah (d) and the median soil moisture value based on 16 chosen GCM outputs.

can be evaluated (Wang *et al* 2010). More detailed information about the algorithms can be found in Wang *et al* (2010).

$$P_{D,G} = 1 - \frac{1}{{\sigma_G}^2} \sum_{i=1}^{m} n_{D,i} {\sigma_{D,i}}^2$$

where $i = 1, 2, \ldots, m$ is each unit of influencing factors; $n_{D,i}$ is the number of units; ${\sigma_G}^2$ and ${\sigma_{D,i}}^2$ are the variance of observed region and each unit. $P_{D,G}$ locates among 0–1, and the more the value of $P_{D,G}$ is, the greater the influence of the factor D on SM). When the $P_{D,G}$ equal closely to 1, that is, $\sum_{i=1}^{m} n_{D,i} {\sigma_{D,i}}^2$ is near to 0, that means the influencing factor has the same spatial patterns with the SM (Wu *et al* 2016).

4. Results and discussions

4.1. Selection and verification of GCMs from CMIP5

Figure 2 shows the ratio of the calibrated trend of historical SM from 25 GCMs to the trend of the GLDAS-Noah SM by the Sen's slope method during 1981–2005 and relevant spatial patterns of SSM trends. In general, the SSM in CMIP5 can be used to further explore the future variation, which performs better than the RZSM. There are 16 models of which the median of the ratios is positive for SSM (figure 2(a)), implying consistent trend directions of SSM in GCMs and GLDAS-Noah in more than half of the grids. Therefore, the median of 16 GCMs was calculated to show the calibrated SSM (figure 2(d)). For the root-zone SM (RZSM, figure 2(b)), there are only nine GCMs for which consistent trend directions were identified at more than half of the grids, which indicates that GCMs have it harder to depict the trends in the RZSM than for SSM. To some extent, the RZSM is difficult to be simulated using modeling techniques such as GCMs in CMIP5 and GLDAS-Noah as well. Meanwhile, the modeled soil depth is heavily model-dependent and varies widely from GCMs. Berg *et al* (2016) found that the maximum monthly SM over the hydrological active layers varies from ~1400 kg m^{-2} for ACCESS1-0 to ~7000 kg m^{-2} for MIROC-ESM. The processing method to integrate RZSM to 2 m depth and the hypothesis of linear variation in the soil layers may also introduce uncertainties and even errors.

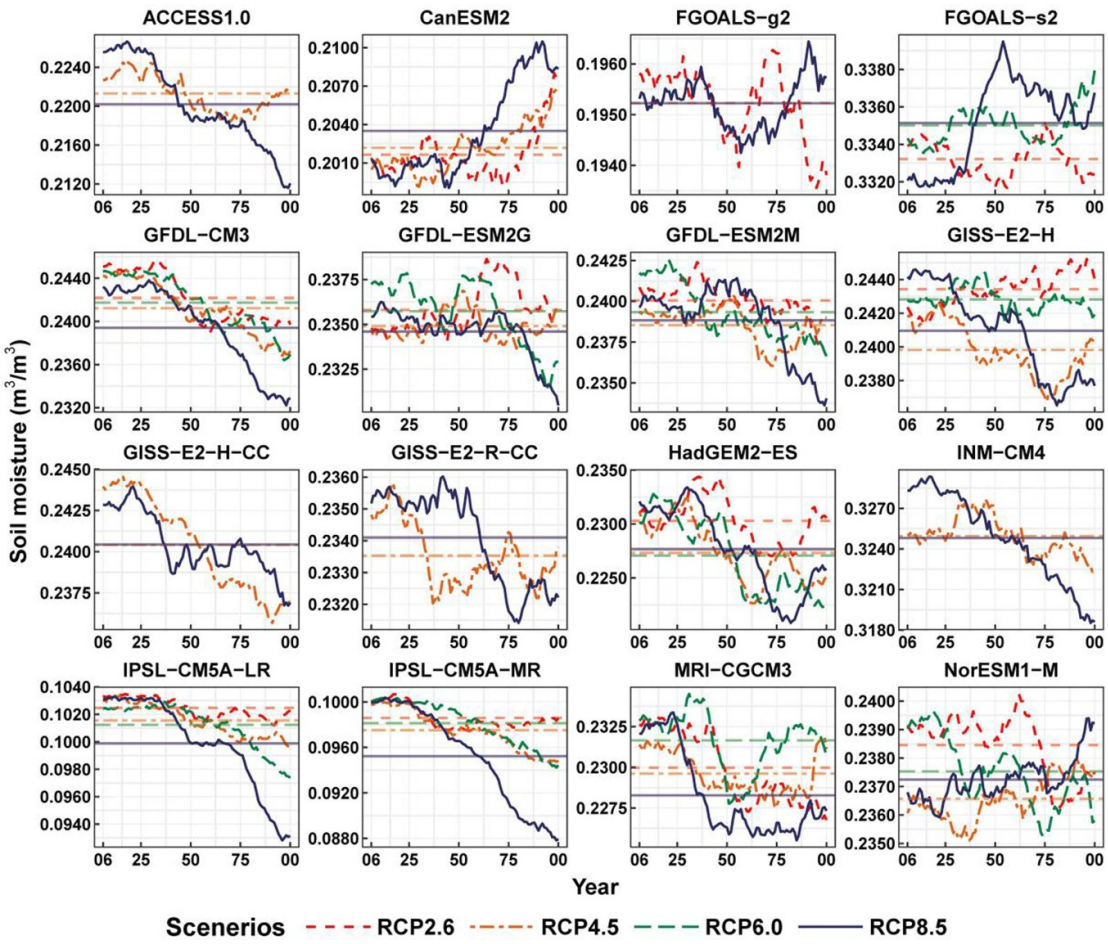

Figure 3. Annual variations of the surface volumetric soil moisture under four scenarios: RCP2.6, RCP4.5, RCP6.0 and RCP8.5. The annual variations of the surface volumetric soil moisture were derived from 20 year moving average of the GCM outputs during 2006–2100. The horizontal line corresponds to the mean value over the whole time period for different scenarios. The individual figures represent the models listed in table 2. Among, the *x*-axis labels: 06, 25, 50, 75 and 00 refer to the year of 2006, 2025, 2050, 2075 and 2100.

The magnitude of trends cannot be well quantified, even the trend direction can be well captured by SSM of GLDAS-Noah and GCMs. The correction factors are 5.64 and 10.32 for the SSM and the RZSM respectively based on the chosen models (16 for SSM; 9 for RZSM, equation (3)). This indicates that the magnitude of the SSM can be predicted with higher accuracy than the RZSM and the GCMs usually underestimate the magnitude of SM change relative to the DLDAS-Noah data. Figure 2(c) shows spatial patterns of SSM trend based on the GLDAS-Noah SSM data and figure 2(d) shows spatial patterns of the calibrated SSM trend based on the GCMs outputs. Magnitude of the SSM trend is $-0.03\ m^3\ m^{-3}\ 100^{-yr}$. We also observed similar SSM trends for GLDAS-Noah and GCMs in most grids across China, and in NEC, CNW, NWC, CCH, SCH, TPC, in particular. Obvious drying trends of GLDAS-Noah SSM are $-0.015\ m^3\ m^{-3}\ 100^{-yr}$ in ENW and $-0.013\ m^3\ m^{-3}\ 100^{-yr}$ in NCH, which is similar to the standing results (Dorigo *et al* 2012). However, wetting trends were found for SSM in ENW and NCH with magnitude of $0.015\ m^3\ m^{-3}\ 100^{-yr}$ and $0.007\ m^3\ m^{-3}\ 100^{-yr}$, respectively. Moreover, wetting tendency was found in WNW based on GCMs outputs with magnitude of $0.002\ m^3\ m^{-3}\ 100^{-yr}$. While most regions in WNW are in drying tendency based on GLDAS-Noah dataset with magnitude of $-0.004\ m^3\ m^{-3}\ 100^{-yr}$.

4.2. Future SSM changes based on GCM outputs

Figure 3 illustrates the annual change of the volumetric moisture content for SSM under four scenarios: RCP2.6, RCP4.5, RCP6.0 and RCP8.5 covering 2006–2100, which has been calculated by moving average. Projection results indicate that SSM outputs of more than half of 16 models are in drying trend for all scenarios considered in this study, by which the drying trend is acceptable in the future. Feng and Fu (2013) and Dai (2013) advocated that, in the backdrop of global warming, the arid areas in many lands have expanded and will continue to be expanding in the next century. Meanwhile, the results of different models are discrepant, even the GCMs have been selected by certain criteria and the SSM based on CMIP5 outputs is comparable in quantity (Berg *et al* 2016). The averaged SSM based on most GCMs outputs is around 0.20–0.25 $m^3\ m^{-3}$.

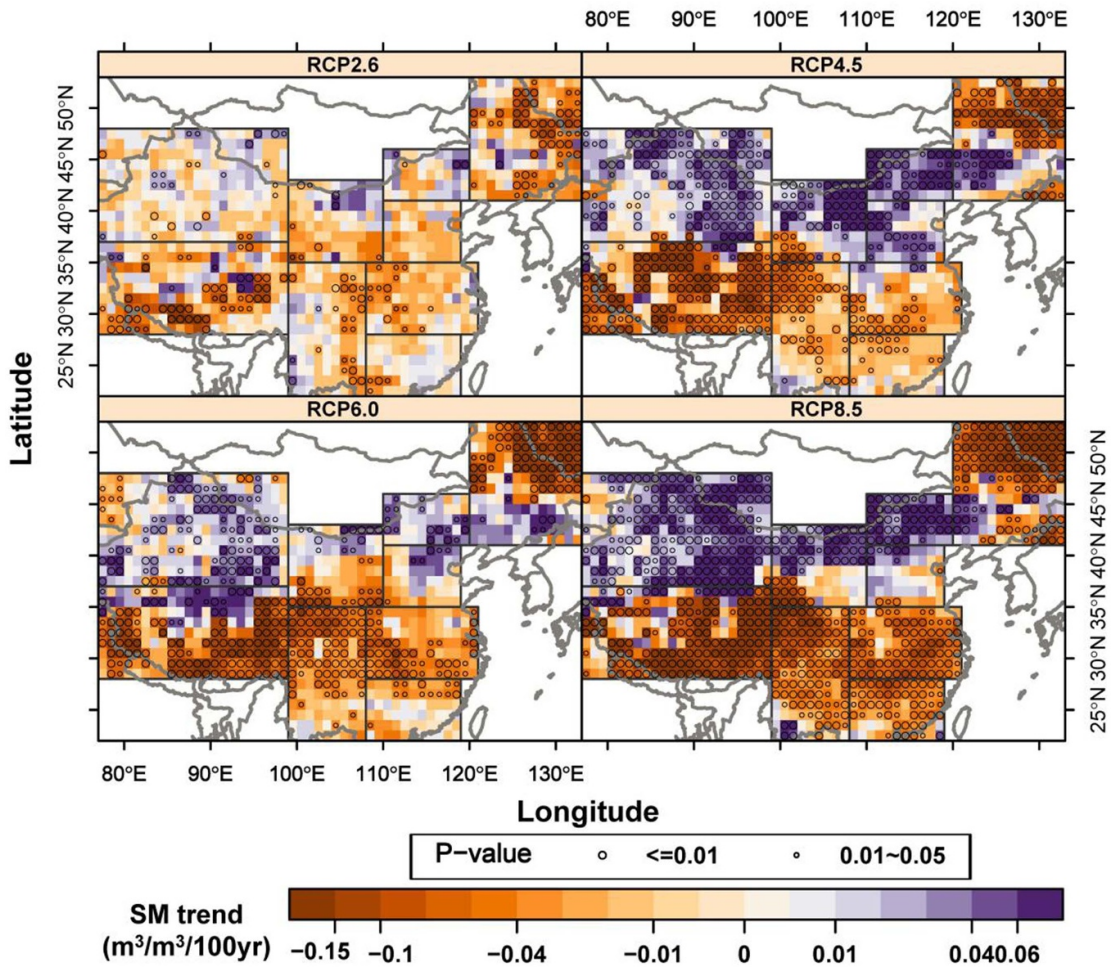

Figure 4. Trend and *P*-value of SSM change under different scenarios calculated by Sen's Slope method. The colored tape indicates the magnitude of trend of SM change relative to the baseline period of 1981–2005.

However, SSM outputs by FGOALS-s2 and INM-CM4 predicts the SSM of ∼0.33 m^3 m^{-3} above the mean value, and SSM outputs by IPSL-CM5A-LR and IPSL-CM5A-MR predict the SSM of ∼0.10 m^3 m^{-3} below the mean value. Lu *et al* (2019) found that the uncertainty of future SM projection is mainly determined by models, compared with the uncertainty from the global decadal annual temperature changes (Hawkins and Sutton 2009). Under RCP8.5 scenario, SSM of 12 GCMs is in obvious drying tendency. Nearly half of models identify that, under RCP8.5 scenario, the surface soil layer displays less mean SM content than other scenarios, as a contrast, and the models display different features for different scenarios. Generally, the warmer the climate, the drier the SSM. Lu *et al* (2019) found that the average annual SM in the 21st century shows significantly large-scale drying and wetting tendency in a limited area under all scenarios, and the stronger radiative forcing brings stronger drying tendency, which is consistent with our findings.

Throughout the whole future periods (2006–2100) in CMIP5 simulations, the spatial patterns of SSM changes are basically similar, that is, wetting SSM in WNW, CNW, ENW, NCH and south of NEC, and drying SSM in the other regions (figure 4). From lower to higher emission scenarios, the magnitude of SSM changes gradually increases and more grids are characterized by significant SSM changes. But SSM changes under RCP6.0 scenario do not conform to this pattern. Under RCP2.6 scenario, the magnitude of SSM change is not evident and a drying SSM trend can be found in 66.8% of mainland China (15.4% with <0.05 *P*-value, 7.9% with <0.01 *P*-value). Comparatively, wetting SSM trends were identified in 33.2% of mainland China (2.8% with <0.05 *P*-value, 1.2% with <0.01 *P*-value). Also, substantial spatial heterogeneity of SSM changes across China was found, implying no obviously consistent SSM changes under RCP2.6 scenario relative to those under other scenarios. Under RCP8.5 scenario, drying SSM trends were detected across 56.9% of China (44.2% with <0.05 *P*-value, 38.0% with <0.01 *P*-value). Contrastively, wetting SSM trends were observed across 43.1% of China (29.4% with <0.05 *P*-value, 25.1% with <0.01 *P*-value). Considerable spatial heterogeneity in SSM changes can also be observed across different regions of China. However,

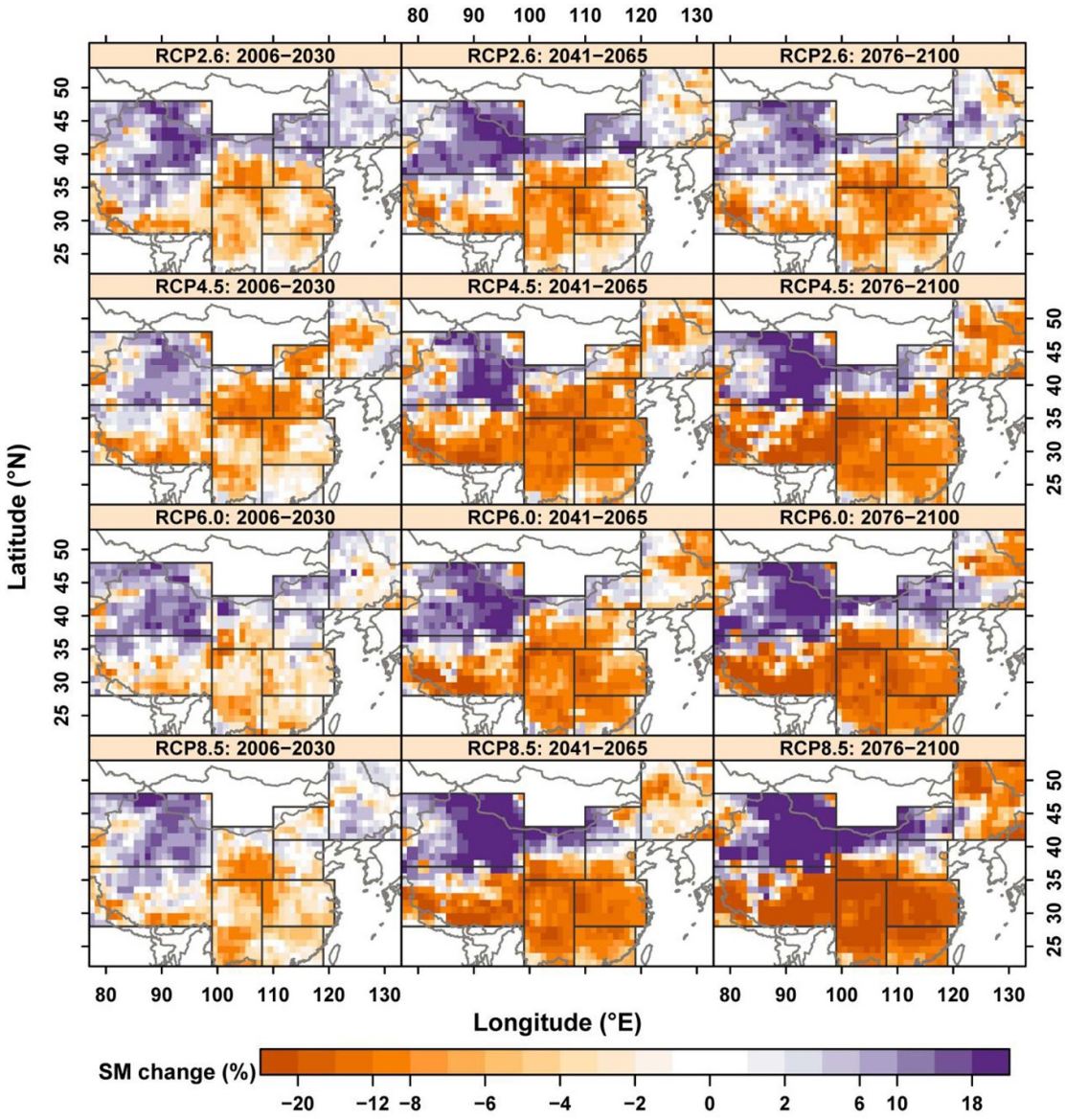

Figure 5. Multi-model (16) median of SSM change percentage for 2005–2030, 2041–2065 and 2076–2100 relative to 1981–2005 under RCP2.6, RCP4.5, RCP6.0 and RCP8.5 scenarios.

confirmative and discernable spatial patterns of SSM changes under RCP8.5 scenario can also be identified with exceptions of CNW and NCH. These results indicated larger area of regions with significant SSM changes given higher temperature. These results are consistent with the findings that the south regions are getting dryer and the north regions except northeast regions are getting wetter in China (Berg *et al* 2016). Moreover, Douville and Plazzotta (2017) found that a summer mid-latitude drying on the northern continents recently appeared at the end of 20th century, which has been attributed to anthropogenic climate change.

4.3. Evolution of relative percentage of SSM under different scenarios

Figure 5 shows the evolution of the multi-model ensemble median of the percentage of SSM change relative to the reference time (1981–2005), which is generally used to explore the past and future SM variations (Rodrigo 2015; Wu *et al* 2015). Generally, SSM changes during the periods of 2006–2030, 2041–2065 and 2076–2100 indicated wetting tendency in arid regions and drying tendency in humid regions. Specifically, most regions in WNW are getting wetter, and wetting tendency can also be found in the north parts of CNW and the northwest parts of ENW. The south parts of China are getting drier where there are naturally humid regions.

Under RCP2.6 scenario, the north China including WNW, TPC, NEC, ENW and north of CNW are getting wetter, and in WNW particularly during 2006–2030. The period of 2041–2065 witnessed shrinking regions with wetting tendency to north and west such as WNW, ENW and north of CNW. The period of 2076–2100 was characterized by drying

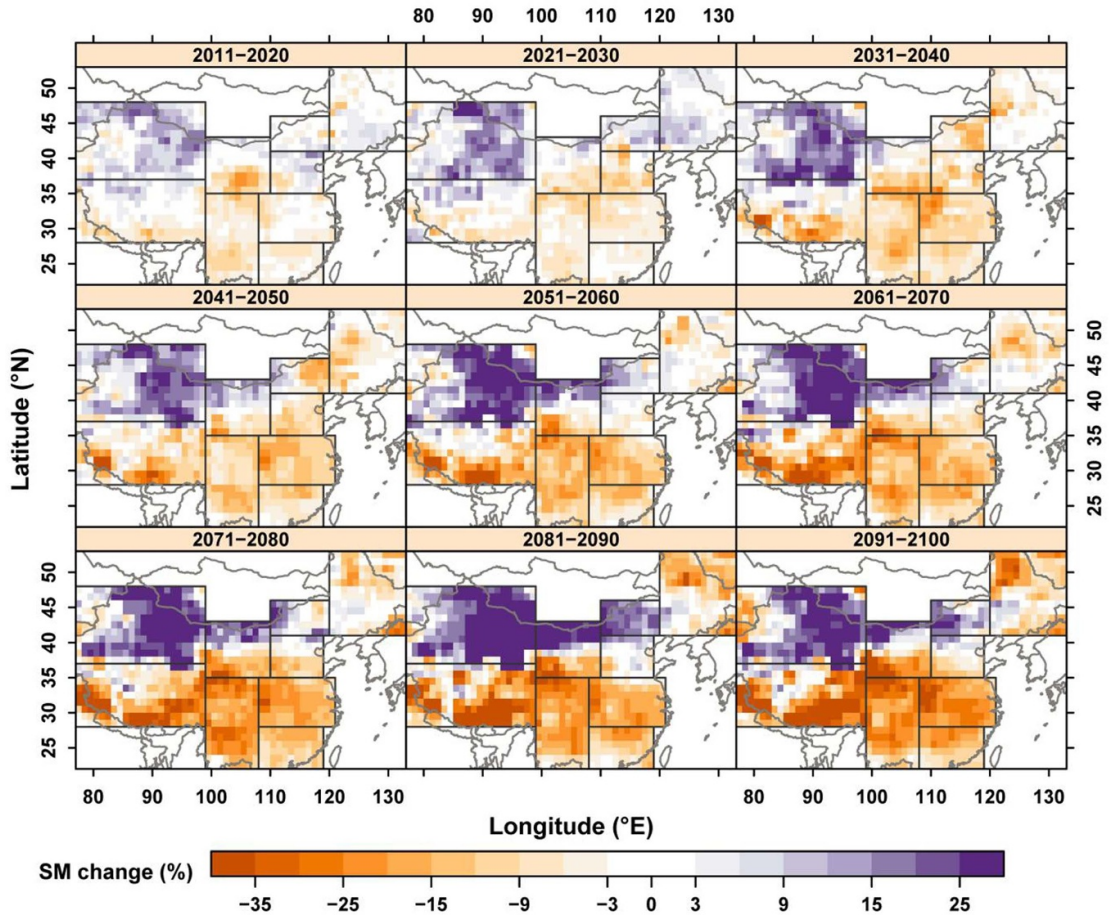

Figure 6. Spatial evolution of the SSM change under RCP8.5 scenario. The multi-model (16) median of the soil moisture change relative to the benchmark period was displayed in every following 10 years.

tendency across the entire China. Relative to area and magnitude of wetting tendency during 2041–2065, the area and magnitude of wetting tendency shrink during 2076–2100. Meanwhile, the bounds and magnitude of drying tendency are expanding. Wherein, the obviously drying regions can be observed in the northwestern part of CCH. Under RCP4.5 scenario, the wetting tendency can be found in WNW during 2006–2030 and 2041–2065 and gradually extends to CNW during 2076–2100. However, regions with appreciable drying tendency move westwards till to the TPC. Under RCP6.0 scenario, the WNW is dominated by wetting tendency. The north China is dominated by wetting tendency during 2006–2030, by drying tendency during 2041–2065 and again by wetting tendency during 2076–2100. Consistent drying tendency can be found in the south China. Under RCP8.5 scenario, magnitude of SSM change continues to increase, i.e. the dry-wetter and wet-drier scheme.

For cold regions like NEC and TPC, wetting trend is detected during 2006–2030 and followed by a sharp drying trend under RCP6.0 and RCP8.5 scenarios. Under these scenarios, the persistently rising air temperature gives rise to melting of glaciers, snow cover and permafrost in NEC and TPC. In WNW, the increased SSM is observed during historical period relative to the reference period. The discrepancy in the SSM projections under these four scenarios considered in this study is quite small during the period of 2006–2030 due to the similar radiative forcing during this period (Meinshausen *et al* 2011). During 2041–2065, from RCP2.6, RCP4.5, RCP6.0 to RCP8.5 scenarios, the drying amplitude of the SSM gradually increases, drying amplitude of SSM under RCP6.0 scenario is smaller than that under RCP4.5 scenario which is related to the radiative forcings under different scenarios. RCP8.5 is referred to the highest radiative forcing scenario, and RCP2.6 is the lowest radiative forcing scenario in the following century. But in the near future, approximately by the year of 2050, the radiative forcing under RCP4.5 is higher than that under RCP6.0, that is adverse in the long-term future (Masui *et al* 2011, Nazarenko *et al* 2015).

Here we also presented the evolution process of SSM to explore the SM variation at shorter time step under RCP8.5 scenario and the SM variation of each 10 years was displayed (figure 6). RCP8.5, as the highest radiative forcing, will bring to a strongest global warming related with other scenarios (Riahi *et al* 2011). But we found that the trends of SM variation in the same one place during different future

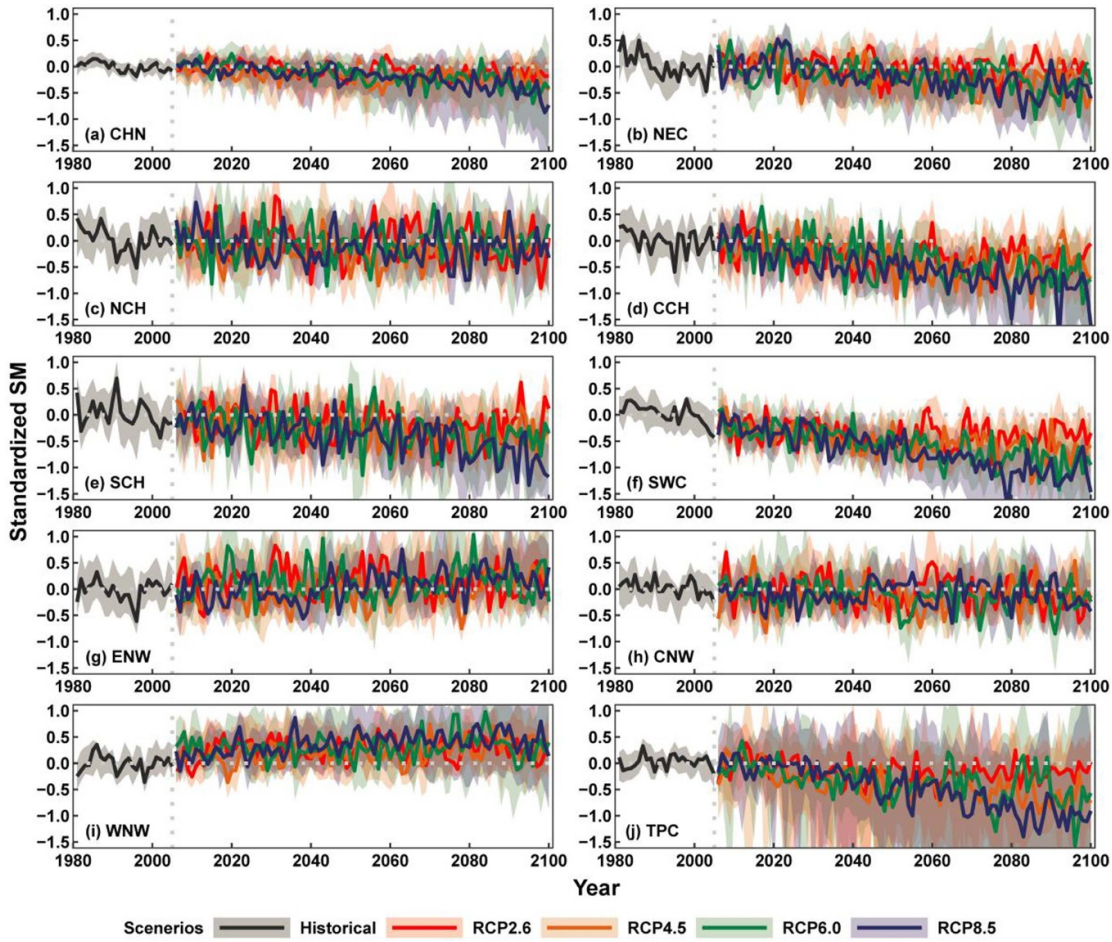

Figure 7. Temporal variations of the standardized surface soil moisture in the past periods and in the future under different scenarios (historical, RCP2.6, RCP4.5, RCP6.0, RCP8.5). The surface soil moisture was standardized by the mean surface soil moisture during 1981–2005. The hard line shows the multi-model median of 25 models. The shadow indicates the 90% confidence interval of 25 model predictions.

periods are different even under the highest radiative forcing scenarios, RCP8.5. It can be seen from figure 6 that SSM at most of the grids is in consistent changing properties during the entire study period. However, the entire NEC is dominated by wetting SSM during 2011–2030, then by drying SSM during 2030–2080. During 2081–2100, SSM variation is subject to discernable spatial heterogeneity in NEC, SSM in most grids continues to decrease and increased SSM can be observed in the southwest of NEC.

Figure 7 shows the temporal variations of the standardized SSM during 1981–2100. SSM overall is in a downward trend across the entire mainland China under all scenarios considered in this study, indicating a drying tendency in the future under RCP8.5 scenario in particular. In WNW, increased SSM during in 2005–2035 is observed. A wetting trend in SSM variability can be identified during 2036–2100, highlighting the possibility for increased frequencies of extremely dry and wet spells. In ENW, there is a slightly wetting SSM trend in the future. Besides, NEC, CCH, SCH, SWC and TPC witness a significant drying SSM in the future (figure 6). Interesting is that the period of 2005–2100 shows no obvious trend in NCH and CNW; however, the variabilities are increasing. Figures 5 and 6 illustrate significant spatial heterogeneity of SSM in NCH and CNW and nearly half of the area shows different changing features of SSM.

4.4. Attribution of meteorological variables to SSM variations

Meteorological variables having potential impacts on SSM are precipitation, temperature, relative humidity and wind speed (Deng *et al* 2020). Precipitation amount has direct impacts on SSM changes, with the relative contribution of up to 43.4% to SSM variations (table 3) due to the most important supply from precipitation for most regions which is consistent with the previous findings all over the world in the past period (e.g. Deng *et al* 2020). Temperature, wind speed and relative humidity have the relative contribution of 22.5%, 19.9% and 14.2% respectively (table 3) which all can change SSM content by soil evaporation and vegetation transpiration, among them, temperature have greater impacts on evapotranspiration under global warming (Deng *et al* 2020).

Table 3. The relative contribution (%) of relative humidity (a), wind speed (b), temperature (c) and precipitation (d) calculated to surface soil moisture changes based on Geodetector method in different regions of China under the RCP8.5 scenario.

Variables	CHN	NEC	NCH	CCH	SCH	SWC	ENW	CNW	WNW	TPC
Precipitation	43.4	39.4	42.6	45.2	45.2	43.1	48.0	41.9	51.1	44.1
Temperature	22.5	27.6	28.5	16.4	18.1	17.7	18.3	14.1	14.7	16.4
Wind	19.9	17.7	13.0	13.8	20.5	18.8	16.6	21.8	16.1	17.7
Humidity	14.2	15.3	15.8	24.7	16.2	20.3	17.2	22.2	18.1	21.9

We found different impacts of these meteorological factors on SSM changes. Specifically, SSM in the WNW is mainly influenced by precipitation changes with relative contribution of 51.1% (table 3). SSM in NCH is affected by the temperature changes with relative contribution of 28.5% (table 3) due to the fact that a sharp rise of temperature can affect SSM content by modifying evapotranspiration processes. Meanwhile, evapotranspiration also affects precipitation by changing water vapor transportation to the atmosphere (Oki and Kanae 2006). It was evidenced that SSM is in negative relation with temperature (Cheng and Huang 2016, Deng *et al* 2020). Besides, SSM changes in CNW and CCH are affected mainly by the wind speed and the relative humidity with relative contribution of 21.8% and 24.7% respectively to SSM changes. The results show that the SSM change is affected by the combination of meteorological factors, except these, the vegetation and agricultural activities in the future also have great impacts on SSM changes (Liu *et al* 2015, Deng *et al* 2020).

5. Conclusions

We thoroughly analyzed spatiotemporal patterns of SSM across mainland China and the relevant influencing factors behind the variations in SSM. The following findings and conclusions are obtained:

(a) The direction of the historic trends of SSM during 1981 and 2005 can be well captured by 16 out of the 25 CMIP5 GCMs. The historic simulation and future projections of SSM for these 16 models provides the basis for further analysis. The SSM data for the historic period by the GLDAS-Noah was used to calibrate the magnitudes of the corresponding SSM trends estimated by the selected 16 models with satisfactory performance. The calibration is then used for future GCM projections under four IPCC emission scenarios.

(b) Under RCP2.6 scenario, SSM has no significant change in most regions across China. But under the other three emission scenarios, arid and semi-arid regions are dominated by wetting SSM and vice versa. The higher the global temperature rises, the more grids with significant changes and larger magnitude of SSM changes. Under RCP8.5 scenario, drying SSM can be found in 56.9% of regions across China (44.2% with <0.05 *P*-value). As a comparison, wetting SSM trends can be observed in 43.1% of the regions across mainland China (29.4% with <0.05 *P*-value).

(c) For all regions considered, precipitation is the most important factor for SSM variations among the four meteorological variables considered. On average, its relative contribution to SSM variation can reach over 43.4%. Temperature, wind speed and relative humidity have relative contributions of 22.5%, 19.9% and 14.2% to SSM changes respectively. There is a small difference in the relative contributions of the four variables among the regions.

Data availability statement

The data that support the findings of this study are available upon reasonable request from the authors.

Acknowledgments

This research has been supported by the China National Key R&D Program, Grant No. 2019YFA 0606900, the National Science Foundation of China, Grant No. 41771536, and the National Science Foundation for Distinguished Young Scholars of China, Grant No. 51425903. All authors declare no conflict of interest. Our cordial gratitude should be extended to the editor, Professor Dr Freddie Taylor, Professor Dr Johnathan Keen and anonymous reviewers for their professional and pertinent comments which are greatly helpful for further quality improvement of this current manuscript. We would like to thank the high-performance computing support from the Center for Geodata and Analysis, Faculty of Geographical Science, Beijing Normal University (https://gda.bnu.edu.cn/).

Author contributions

QZ designed the research with input from DC; KF performed analysis; QZ, KF, and PL wrote the paper; DC and CYX reviewed and improved the paper; PS, XZ, HY, ZS, and PH contributed new analytic tools and performed analyses.

Conflict of interest

The authors declare no conflict of interest.

ORCID iD

Jianping Li https://orcid.org/0000-0003-0625-1575

References

Albergel C, Dorigo W, Reichle R H, Balsamo G, De Rosnay P, Munoz-Sabater J, Isaksen L, De Jeu R and Wagner W 2013 Skill and global trend analysis of soil moisture from reanalysis and microwave remote *J. Hydrometeorol.* **14** 1259–77

Berg A *et al* 2016 Land-atmosphere feedbacks amplify aridity increase over land under global warming *Nat. Clim. Change* **6** 869–74

Berg A, Sheffield J and Milly P C D 2017 Divergent surface and total soil moisture projections under global warming *Geophys. Res. Lett.* **44** 236–44

Brocca L, Moramarco T, Melone F, Wagner W, Hasenauer S and Hahn S 2012 Assimilation of surface- and root-zone ASCAT soil moisture products into rainfall-runoff modeling *IEEE Trans. Geosci. Remote Sens.* **50** 2542–55

Cao F, Ge Y and Wang J F 2013 Optimal discretization for geographical detectors-based risk assessment *GISci. Remote Sens.* **50** 78–92

Chen T, De Jeu R A, Liu Y Y, Der Werf G R and Dolman A J 2014 Using satellite based soil moisture to quantify the water driven variability in NDVI: a case study over mainland Australia *Remote Sens. Environ.* **140** 330–8

Chen X, Liu X, Liu Z, Zhou P, Zhou G, Liao J and Liu L 2016b Spatial clusters and temporal trends of seasonal surface soil moisture across China in responses to regional climate and land cover changes *Ecohydrology* **10** e1800

Chen X, Su Y, Liao J, Shang J, Dong T, Wang C, Liu W, Zhou G and Liu L 2016a Detecting significant decreasing trends of land surface soil moisture in eastern China during the past three decades (1979–2010) *J. Geophys. Res. Atmos.* **121** 5177–92

Cheng S and Huang J 2016 Enhanced soil moisture drying in transitional regions under a warming climate *J. Geophys. Res. Atmos.* **121** 2542–55

Cui Y, Zeng C, Zhou J, Xie H, Wan W, Hu L, Xiong W, Chen X, Fan W and Hong Y 2019 A spatio-temporal continuous soil moisture dataset over the Tibet Plateau from 2002 to 2015 *Sci. Data* **6** 1–7

Dai A 2013 Increasing drought under global warming in observations and models *Nat. Clim. Change* **3** 52–58

Deng Y *et al* 2020 Variation trend of global soil moisture and its cause analysis *Ecol. Indic.* **110** 105939

Dorigo W, De Jeu R, Chung D, Parinussa R, Liu Y Y, Wagner W and Fernandezprieto D 2012 Evaluating global trends (1988–2010) in harmonized multi-satellite surface soil moisture *Geophys. Res. Lett.* **39** L18405

Douville H and Plazzotta M 2017 Midlatitude summer drying: an underestimated threat in CMIP5 models? *Geophys. Res. Lett.* **44** 9967–75

Fan K, Zhang Q, Singh V P, Sun P, Song C, Zhu X, Yu H and Shen Z 2019 Spatiotemporal impact of soil moisture on air temperature across the Tibet Plateau *Sci. Total Environ.* **649** 1338–48

Feng H and Liu Y 2015 Combined effects of precipitation and air temperature on soil moisture in different land covers in a humid basin *J. Hydrol.* **531** 1129–40

Feng S and Fu Q 2013 Expansion of global drylands under a warming climate *Atmos. Chem. Phys.* **13** 10081–94

Gu X, Zhang Q, Li J, Singh V P, Liu J, Sun P and Cheng C 2019 Attribution of global soil moisture drying to human activities: a quantitative viewpoint *Geophys. Res. Lett.* **46** 2573–82

Guillod B P, Orlowsky B, Miralles D G, Teuling A J and Seneviratne S I 2015 Reconciling spatial and temporal soil moisture effects on afternoon rainfall *Nat. Commun.* **6** 6443

Gunda T, Nawagamuwa U P and Hornberger G M 2017 Combined impact of local climate and soil properties on soil moisture patterns *Hydrol. Earth Syst. Sci. Discuss.* **21** 1–22

Hauser M, Orth R and Seneviratne S I 2016 Role of soil moisture versus recent climate change for the 2010 heat wave in western Russia *Geophys. Res. Lett.* **43** 2819–26

Hawkins E and Sutton R 2009 The potential to narrow uncertainty in regional climate predictions *Bull. Am. Meteorol. Soc.* **90** 1095–108

Huang J, Yu H, Guan X, Wang G and Guo R 2016 Accelerated dryland expansion under climate change *Nat. Clim. Change* **6** 166–71

Koster R D *et al* 2004 Regions of strong coupling between soil moisture and precipitation *Science* **305** 1138–40

Koster R D, Guo Z, Yang R, Dirmeyer P A, Mitchell K and Puma M J 2009 On the nature of soil moisture in land surface models *J. Clim.* **22** 4322–35

Lawrence D M *et al* 2011 Parameterization improvements and functional and structural advances in version 4 of the community land model *J. Adv. Model. Earth Syst.* **3** M03001

Liu Y *et al* 2015 Agriculture intensifies soil moisture decline in Northern China *Sci. Rep.* **5** 11261

Liu Y, Liu Y and Wang W 2019 Inter-comparison of satellite-retrieved and Global Land Data Assimilation System-simulated soil moisture datasets for global drought analysis *Remote Sens. Environ.* **220** 1–18

Lu J, Carbone G J and Grego J M 2019 Uncertainty and hotspots in 21st century projections of agricultural drought from CMIP5 models *Sci. Rep.* **9** 1–12

Masui T, Matsumoto K, Hijioka Y, Kinoshita T, Nozawa T, Ishiwatari S, Kato E, Shukla P R, Yamagata Y and Kainuma M 2011 An emission pathway for stabilization at 6 Wm^{-2} radiative forcing *Clim. Change* **109** 59–76

McColl K A, Alemohammad S H, Akbar R, Konings A G, Yueh S and Entekhabi D 2017 The global distribution and dynamics of surface soil moisture *Nat. Geosci.* **10** 100–4

Meinshausen M *et al* 2011 The RCP greenhouse gas concentrations and their extensions from 1765 to 2300 *Clim. Change* **109** 213–41

Miralles D G *et al* 2014 El Niño-La Niña cycle and recent trends in continental evaporation *Nat. Clim. Change* **4** 122–6

Miralles D G, Gentine P, Seneviratne S I and Teuling A J 2019 Land-atmospheric feedbacks during droughts and heatwaves: state of the science and current challenges *Ann. New York Acad. Sci.* **1436** 19–35

Miralles D G, Holmes T R, Jeu D R, Gash J H, Meesters A G and Dolman A J 2010 Global land-surface evaporation estimated from satellite-based observations *Hydrol. Earth Syst. Sci.* **15** 453–69

Nazarenko L *et al* 2015 Future climate change under RCP emission scenarios with GISS ModelE2 *J. Adv. Model. Earth Syst.* **7** 244–67

Oki T and Kanae S 2006 Global hydrological cycles and world water resources *Science* **313** 1068–72

Riahi K, Rao S, Krey V, Cho C, Chirkov V, Fischer G, Kindermann G, Nakicenovic N and Rafaj P 2011 RCP 8.5–a scenario of comparatively high greenhouse gas emissions *Clim. Change* **109** 33

Rodell M *et al* 2004 The global land data assimilation system *Bull. Am. Meteorol. Soc.* **85** 381–94

Rodrigo F S 2015 On the covariability of seasonal temperature and precipitation in Spain, 1956–2005 *Int. J. Climatol.* **35** 3362–70

Samaniego L, Thober S, Kumar R, Wanders N, Rakovec O, Pan M, Zink M, Sheffield J, Wood E F and Marx A 2018 Anthropogenic warming exacerbates European soil moisture droughts *Nat. Clim. Change* **8** 421–6

Stocker T F *et al* 2013 *Climate Change 2013: The Physical Science Basis. Contribution of Working Group I to the Fifth Assessment Report of the Intergovernmental Panel on Climate Change* (Cambridge and New York: Cambridge University Press) (https://doi.org/10.1017/CBO9781107415324)

Taylor K E, Balaji V, Hankin S, Juckes M, Lawrence B and Pascoe S 2012 CMIP5 data reference syntax (DRS) and controlled

vocabularies (www.medcordex.eu/cmip5_data_reference_syntax.pdf)
Varallyay G 2010 The impact of climate change on soils and on their water management *Agron. Res.* **8** 385–96 (https://agronomy.emu.ee/vol08Spec2/p08s214.pdf)
Wang A, Lettenmaier D P and Sheffield J 2011 Soil moisture drought in China, 1950–2006 *J. Clim.* **24** 3257–71
Wang G 2005 Agricultural drought in a future climate: results from 15 global climate models participating in the IPCC 4th assessment *Clim. Dyn.* **25** 739–53
Wang J, Li X, Christakos G, Liao Y, Zhang T, Gu X and Zheng X 2010 Geographical detectors-based health risk assessment and its application in the neural tube defects study of the Heshun region, China *Int. J. Geogr. Inf. Sci.* **24** 107–27
Wu F, Zhan J, Su H, Yan H and Ma E 2015 Scenario-based impact assessment of land use/cover and climate changes on watershed hydrology in Heihe River Basin of northwest China *Adv. Meteorol.* **2015** 410198
Wu R, Zhang J, Bao Y and Zhang F 2016 Geographical detector model for influencing factors of industrial sector carbon dioxide emissions in Inner Mongolia, China *Sustainability* **8** 149
Xiao M, Zhang Q, Singh V P and Chen X 2013 Regionalization-based spatiotemporal variations of precipitation regimes across China *Theor. Appl. Climatol.* **114** 203–12
Yu H, Zhang Q, Xu C-Y, Du J, Sun P and Hu P 2019 Modified palmer drought severity index: model improvement and application *Environ. Int.* **130** 104951
Zhang Q, Fan K, Singh V P, Song C, Xu C Y and Sun P 2019 Is Himalayan-Tibetan Plateau 'drying'? Historical estimations and future trends of surface soil moisture *Sci. Total Environ.* **658** 374–84
Zhang Q, Fan K, Singh V P, Sun P and Shi P 2018 Evaluation of remotely sensed and reanalysis soil moisture against *in situ* observations on the Himalayan-Tibetan Plateau *J. Geophys. Res. Atmos.* **123** 7132–48
Zhang Q, Gu X, Singh V P, Kong D and Chen X 2015 Spatiotemporal behavior of floods and droughts and their impacts on agriculture in China *Glob. Planet. Change* **131** 63–72
Zhang Q, Zheng Y, Singh V P, Luo M and Xie Z 2017 Summer extreme precipitation in eastern China: mechanisms and impacts *J. Geophys. Res. Atmos.* **122** 2766–78
Zhao T and Dai A 2015 The magnitude and causes of global drought changes in the twenty-first century under a low-moderate emissions scenario *J. Clim.* **28** 4490–512
Zohaib M, Kim H and Choi M 2017 Evaluating the patterns of spatiotemporal trends of root zone soil moisture in major climate regions in East Asia *J. Geophys. Res. Atmos.* **122** 7705–22